AIAA 93-3277
Active Control of Oscillatory Lift Forces on a Circular Cylinder

D. Ladd, D. Park, and E. Hendricks
Naval Command, Control and Ocean Surveillance Center, RDT&E DIV
San Diego, CA

N. Nosseir
San Diego State University
San Diego, CA

AIAA
Shear Flow Conference
July 6-9, 1993 / Orlando, FL

ACTIVE CONTROL OF OSCILLATORY LIFT FORCES ON A CIRCULAR CYLINDER

D. M. Ladd*, D. S. Park, E. W. Hendricks
NCCOSC RDT&E DIV 574
San Diego, CA

N. S. Nosseir†
San Diego State Un.
San Diego, CA

Abstract

The results of a computational and experimental study of feedback control of Karman vortex shedding behind a circular cylinder are presented. The experiments were performed in a nominally two dimensional flow around a 12.7mm cylinder at Reynolds numbers up to 10,000. The computations utilized the two-dimensional Navier-Stokes equations at Reynolds numbers up to 100. In both experimental and numerical studies blowing and suction slots were used to control the vortex shedding. In the numerical study complete suppression of vortex shedding is achieved up to a Reynolds number $Re = 80$ (about 70% above the onset Reynolds number for vortex shedding). In the experimental study using the fluctuating lift force as feedback, about 50% suppression of the rms fluctuations has been achieved at a Reynolds number of approximately 10,000.

Nomenclature

C_L	lift coefficient, $L/(0.5\rho d l {U_\infty}^2)$
d	cylinder diameter
$\vec{e}_1$	unit vector in the x direction
$\vec{e}_2$	unit vector in the y direction
f	frequency (Hz)
$k(t)$	feedback function
L	lift force
l	cylinder span
n	vortex shedding frequency (Hz)
Re	Reynolds number, $U_\infty d/\nu$
St	Strouhal number, nd/U_∞
t	time
$\vec{u}$	velocity vector normalized by U_∞
u_Γ	blowing/suction normalized velocity (Numerical solution)
U_∞	freestream velocity
v	peak velocity of blowing/suction (experiment)
x, y	coordinate system, centered on cylinder axis, x aligned with U_∞
x_s	vertical velocity sensor location
α	feedback gain
ν	kinematic viscosity
ρ	fluid density
θ	azimuthal angle
τ	time (prior to t)

*Member AIAA
†Professor, Aerospace Engineering, Member AIAA

1 Introduction

Many flows of engineering interest (e.g. separating flows) produce the phenomena of vortex shedding and the associated structural response. Applications include marine structures, underwater acoustics, civil and wind engineering to name a few. The ability to tailor the wake of a bluff body could be used to reduce drag, increase mixing or heat transfer and enhance combustion. Vortex shedding from bluff bodies has been reviewed most recently by Sarpkaya [1] and Bearman [2]. Vortex shedding from a cylinder occurs over wide range of Reynolds number from $47 < Re < 300,000$ and then again at $Re > 3\text{x}10^6$. From a mechanistic (perhaps simplistic) point of view, a flow-induced feedback causes the shedding of the vortices, where the changing location of boundary layer separation on one side of the cylinder causes a change in pressure distribution that forces an opposite asymmetric change in boundary separation. Any small flow perturbation is enough to cause the initial asymmetry that starts the feedback mechanism. The observation that the vortex shedding is caused by the moving location of boundary layer separation is supported by the absence of a distinct shedding frequency in the range $300,000 < Re < 3\text{x}10^6$. In this regime, apparently laminar separation followed by turbulent reattachment fixes the turbulent separation location so firmly that feedback is inhibited.

The important aspect of this phenomenon, from a control standpoint, is that the large pressure forces,

both lift and drag, are a result of the small viscous forces acting in the boundary layer of the cylinder. This implies that small control forces applied to the boundary layer can be used to control the larger pressure forces to achieve the effect of modifying the vortex generation and unsteady lift forces.

There have been many papers on the subject of *active open* loop control of vortex shedding behind a bluff body such as Koopmann [3], Griffin & Ramberg [4], Armstrong et al. [5] and Ongoren & Rockwell [6, 7] to name a few. Vortex shedding lock-in usually occurs when a cylinder is oscillated in-line to the flow direction near the natural vortex shedding frequency. However, for the transverse oscillation of the cylinder, vortex shedding lock-in occurs near twice the natural vortex shedding frequency. Vortex lock-in and control of the near-wake can also be observed with small rotational oscillation of a circular cylinder as demonstrated by Tokumaru & Dimotakis [8], Filler et al. [9], Mo [10] and Chen et al. [11]. Blevins [12], Detemple-Laake & Eckelmann [13], Ffowcs Williams & Zhao [14] and Roussopoulos [15] have used acoustic forcing as a means to control vortex shedding.

While there has been an enormous amount of effort put into the study of the open loop control of vortex shedding, very little research has been done in the area of the *feedback control of vortex shedding*. Monkewitz [16] investigated the possibility for the feedback control of global oscillations using a Ginzburg-Landau model equation that mimics the fluid system. He finds a "gain window" where a feedback gain with an optimum phase is sufficient to suppress the growth of the most unstable mode, but is still below the critical value at which higher modes are destabilized. This window narrows as the degree of the supercriticality increases and control is typically lost not far beyond critical conditions. Therefore, at higher supercritical Reynolds numbers, the feedback necessary to stabilize the most unstable mode might destabilize the next unstable mode. Monkewitz et al. [17] suppressed vortex shedding at Reynolds number only about 5% above the onset of vortex shedding. Recently, Roussopoulos [15] conducted a similar feedback control experiment but was only able to suppress the vortex shedding at Reynolds numbers about 20% above the onset.

This paper describes two separate approaches to investigating active feedback control of cylinder wakes. The first approach utilizes the computation of a feedback control of Kármán vortex shedding behind a circular cylinder using a single downstream sensor and a pair of blowing/suction actuators at $\pm 110°$ from the forward stagnation line. The second effort is an experiment using feedback from a load cell which measures the oscillating lift forces on a cylinder to control a pair of blowing/suction slots (at $\pm 67.5°$) in flow of a nominal Reynolds number of 10,000.

2 Numerical Formulation

We solve the following Navier-Stokes equations:

$$\frac{\partial \vec{u}}{\partial t} + \vec{u} \cdot \nabla \vec{u} = -\nabla p + \frac{2}{Re} \nabla^2 \vec{u}, \tag{1}$$

and the continuity equation:

$$\nabla \cdot \vec{u} = 0, \tag{2}$$

where $\vec{u}$ is the normalized velocity vector, and p is the normalized pressure.

The outer boundary condition is

$$\vec{u} = \vec{e}_1 \quad \text{as} \quad |x| \to \infty, \tag{3}$$

and the blowing/suction boundary condition at the cylinder surface is

$$\vec{u}|_{\partial\Omega} = k(t) u_\Gamma(\theta)(\sin\theta \vec{e}_1 + \cos\theta \vec{e}_2), \tag{4}$$

where $\vec{e}_1$ and $\vec{e}_2$ are the unit vectors in the x-direction and y-direction, respectively. The constraint on $u_\Gamma(\theta)$ is

$$\int_0^{2\pi} u_\Gamma(\theta) d\theta = 0, \tag{5}$$

where θ is the azimuthal angle (i.e. mass is conserved). We chose the antisymmetrical blowing/suction velocity profile with respect to the horizontal centerline to control the vortex shedding mode which is antisymmetrical.

The temporal accuracy of the scheme is second order. The computational grid is uniformly stretched in the radial direction such that the grid is denser near the cylinder surface to resolve the high gradient of the flow near the cylinder surface. The outer computational boundary is located at r_∞=116. The number of grid points in circumferential and radial directions are 256 and 150, respectively. The velocities and pressure are expanded in finite Fourier series in the circumferential direction and a second order accurate finite difference method is used in the radial direction. Some of the solutions in section 4 are presented in Park et al. [18]. The readers are referred to this reference and Karniadakis et al. [19] for further details of the numerical method.

3 Experimental Procedure

The experiments for this study were performed in the NCCOSC 12 inch (305mm) Water Tunnel. This tunnel has a round open jet inside an octagonal test section. Models of up to 0.8m length can be accommodated, with flow velocities up to 15m/sec. The tunnel also has

a 24inch (0.6m) butterfly valve which is installed just before the pump. In this study the butterfly valve was used to throttle the flow so that test section velocities as low as 0.1m/sec could be achieved.

The oscillatory lift force on the test cylinder was chosen as the feedback for the control system. A water tunnel is the ideal flow facility for this study since the high density of water produces relatively large lift forces at manageably low shedding frequencies. Figure 1 shows the test cylinder apparatus installed at the exit of the open jet in the NCCOSC water tunnel. The cylinder was 12.7mm in diameter. Lift forces were measured at each end of the cylinder (top and bottom) with custom fabricated load beams. Each beam formed a flexure such that bending the beam in an "S" shape would strain the opposite legs of a four leg Wheatstone bridge strain gage mounted on the beam. Each load beam was assembled in a water proof housing, with the active end of the beam mounted to the end of the cylinder through a rubber rolling seal. The rolling seal acted to keep water out of the housing while permitting a small amount of motion to deflect the load beam. At full load the deflection of the cylinder (perpendicular to the flow direction) was measured to be less than 0.04mm or about 0.3% of the cylinder diameter. The results presented in section 5 were at flow speeds such that lift loads were about 0.1 of the maximum load, so that in this case, the movement of the cylinder in response to the flow is so slight as to be considered insignificant.

Flow visualization, using both hydrogen bubble wire and fluorescein dye with Argon laser (514nm) illumination, showed that the flow was largely coherent across the span, however occasionally a "dislocation" in the shed vortex could be seen. Here "dislocation" refers to a spanwise phase discontinuity of the shed vortex. Later tests using the load cells showed a high coherence between the lift forces measured at the top and bottom load cells (approximately 80%). The aspect ratio (span/diameter) of the test cylinder was 22. With the pictured geometry the Strouhal number of the vortex shedding from the test cylinder was 0.197 and was essentially independent of Reynolds number in the range 1,000-10,000. This is close to but slightly lower than the expected value (0.205). This difference was probably due to the blockage effect of the cylinder in the round jet and the tendency of the Strouhal number to decrease with lower cylinder aspect ratio (Karniadakis & Triantafyllou)[20].

Suction/blowing slots were chosen as actuators. Rotary oscillation may be more effective for a circular cylinder geometry. However, practical design considerations made the rotary actuator too complex, given that lift force needed to be measured also. It was felt that the most effective location for the suction/blowing slots was near to, but upstream of the mean flow separation location on the cylinder. Numerical results for the two-dimensional simulation generally showed this to be true. The mean separation location is Reynolds number dependent, and for the low Reynolds number (80) of the numerical simulation a slot location $\pm 110°$ from the stagnation line was most effective. In the experiment, higher flow velocity corresponding to Reynolds number in the 9,000-10,000 range, was used to get a reasonably large signal on the load cells. The low end response of the load cells was generally limited by vibration from the water tunnel prime mover showing up on the load cell output. At these higher Reynolds numbers the mean separation line wanders about 80° from the forward stagnation line. A slot location of $\pm 67.5°$ was chosen for the experimental cylinder.

Figure 2 is a cross section of the stainless steel cylinder. The cylinder was constructed in two pie shaped sections and then bolted together. Bolt heads (on the aft stagnation line) were filled and faired in to minimize flow disturbance. A distribution manifold for each slot was machined down the length of the larger part, so that pressure drop across the span of the slot was minimized. Also, flow passages feed in from both ends of the cylinder minimizing spanwise flow variations. The slots were created by undercutting the smaller part 0.076mm before assembling the two halves. Imperfect machining created a slot width variation along the span of the cylinder from 0.05mm to 0.10mm, with the worst of the variation at the ends of the cylinder.

Suction/blowing was done by plumbing the slot manifolds to a peristaltic pump located outside the tunnel test section. The pump was connected to a DC servomotor such that a sine wave input to the servoamplifier would produce an oscillatory rotation of the pump. The servomotor/amplifier acted as a velocity servo such that a commanded voltage would produce a corresponding rotational velocity of the motor. The pump motor combination had a generally direct proportional response up to 30Hz. The plumbing was arranged in such a way that the amount of fluid suctioned from one slot would be blown out the opposite slot. Plumbing consisted of as much stiff wall tubing as possible, to minimize the capacitive effect of flexible wall tubing. The peristaltic pump had three pinch rollers bearing on the vinyl tubing that formed the flow circuit. Some flow variation would occur depending on the location of the pinch rollers on the tube relative to the inlet/outlet portion of the pump. This variation was estimated to be as much as 25% for the open loop tests presented in section 5. This variation was averaged over 20 spectrums per forcing frequency for the open loop results presented in figures 6 through 10. For the closed loop tests, a position transducer was added to the pump shaft so that the mean location of the pinch roller could be con-

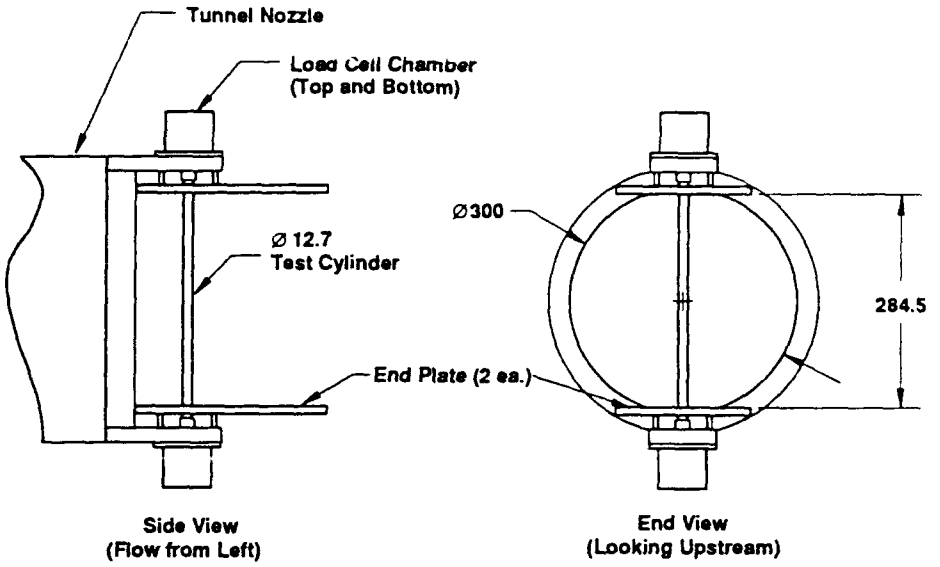

Figure 1: Side and end view of experimental cylinder in NCCOSC Water Tunnel. Dimensions in mm.

trolled. Generally the commanded velocity resulted in only a few degrees (approx. 10) of shaft rotation so the commanded flow is generally directly proportional to shaft rotation in the closed loop case.

4 Numerical Results

Accuracy of the numerical method was validated for the natural vortex shedding case by comparing the numerically obtained Strouhal number St to experimental values at Reynolds numbers 60, 100, 150 and 200. Agreement between our results and the universal $St - Re$ curve of Williamson [21] is excellent (within 2%).

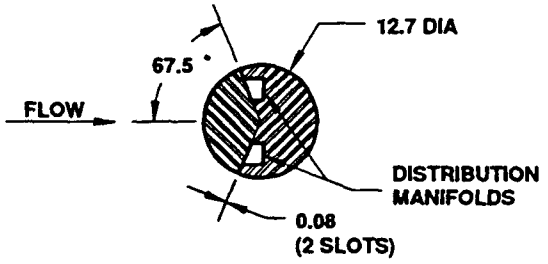

Figure 2: Cross section of test cylinder showing flow passages (manifolds) and slots. Dimensions in mm.

The feedback function $k(t)$ is given by the following formulation:

$$k(t) = \alpha \frac{v(x = x_s, y = 0, t)}{v_{max}(t)}, \tag{6}$$

where

$$v_{max}(t) = \max_{\tau \leq t} |v(x = x_s, y = 0, \tau)|, \tag{7}$$

and $v(x = x_s, y = 0, t)$ is the vertical velocity measured at x=x_s, y=0 at time t,and α is the proportional feedback gain. Changing the sensor location x_s corresponds to changing the phase of the feedback signal. The desired state or goal is to drive or control the flow to the symmetric state with respect to the horizontal centerline, which is the Fornberg's [22] steady solution. Therefore, we chose this forcing function using the vertical velocity at the horizontal centerline since as the desired state (symmetric state) is approached, the required forcing becomes small.

The location of the actuators or the blowing/suction slots is a critical factor in their effectiveness for the suppression of the vortex shedding. Blowing/suction slots at $\pm 50°$, $\pm 65°$,and $\pm 110°$ from the front stagnation of the cylinder were tested. With the actuators

at ±50°, or ±65°, suppression of the vortex shedding was not obtained. We postulate the actuators were ineffective because they were located too far from the separation point on the cylinder surface. The separation points on the cylinder at low Reynolds numbers wander around ±120° as the vortices are shed. When the blowing/suction slots were located at ±110° from the stagnation point, that is slightly ahead of the separation points of the unforced wake, they proved to be strong and effective actuators.

We have achieved the complete suppression of vortex shedding using feedback up to Reynolds number Re=80. The critical Reynolds number for the onset of the vortex shedding is 47. Reynolds number Re=80, is about 70% above the onset Reynolds number and corresponds to the strongly nonlinear state. Monkewitz et al. [17] and Roussopoulos [15] have achieved complete suppression of vortex shedding only up to Reynolds numbers which are about 5% and 10% above the critical onset Reynolds number, respectively.

At Reynolds number Re=80 the suppression of the vortex shedding was achieved with feedback when the sensor was located at x_s=5.5 and the proportional feedback gain α=0.4. The optimum proportional feedback gain α also depends on the width of the blowing/suction slots. The vortex shedding suppression was possible in the narrow range $5.5-\epsilon \leq x_s \leq 5.5+\epsilon$, $0.4-\delta \leq \alpha \leq 0.4+\delta$, where ϵ and δ are small. On the other hand, by reversing the phase of the feedback signal (α=−0.4), keeping x_s same, we were able to enhance the vortex shedding strength and increase the lift force fluctuation amplitude.

Figure 3 is the temporal plot of the lift coefficient and the feedback forcing signal. The time t=0 corresponds to the fully developed natural vortex shedding state. The stabilizing (vortex shedding suppression) feedback forcing (x_s=5.5, α=0.4) is turned on at t=63.7. As one can notice, the lift force fluctuation amplitude decreases from 0.23 to 0.01. The feedback signal starts out at an amplitude of 0.4 (blowing/suction velocity at 40% of the freestream velocity), but goes down to about 0.005 (blowing/suction velocity at 0.5% of the freestream velocity). What is amazing is that such a small amplitude lift force fluctuation level can be maintained with the feedback blowing/suction at mere 0.5% of the freestream velocity. As soon as the feedback forcing is turned off at t=260, the lift force fluctuation begins to increase exponentially and saturate at the natural vortex shedding level.

The flow structures corresponding to vortex shedding, vortex shedding suppression, and vortex shedding enhancement are presented in Figures 4a through 4c. The vorticity plots of Figure 4a-c are all at the same

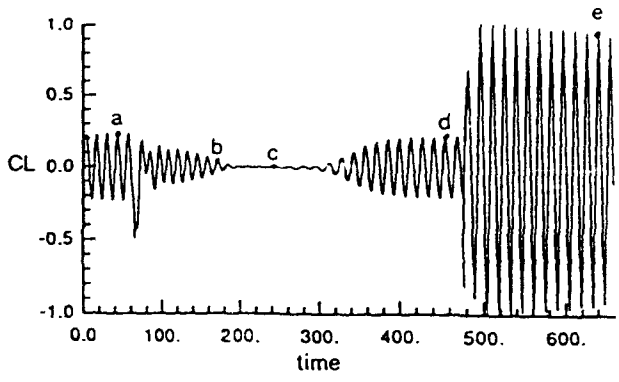

Figure 3: Lift coefficient at Re=80. Stabilizing feedback forcing (x_s=5.5, α=0.4) is turned on at t=63.7 and turned off at t=260. Destabilizing feedback forcing (x_s=5.5, α=-0.4) is turned on at t=475.7. a) t=43.04, b) t=170.9, c) t=243.58, d) t=452.89, e) t=640.3.

phase of the vortex shedding or at the peak of the lift force fluctuation. Figure 4a is the natural vortex shedding. Figure 4b is the reduced vortex shedding state some time after the suppressing feedback forcing is turned on. Note that the vortices being shed are elongated in the streamwise direction. Finally, figure 4c is the fully suppressed state, where the vortex structure looks almost symmetric top and bottom.

The results at slightly higher Reynolds number Re=100 are significantly different. Figure 5 is the lift coefficient plot for the feedback sensor location x_s=5.05 and α=0.3 with slot width slightly larger than that of the Re=80 case. The feedback control is turned on at t=422. Lift fluctuation decreases until t=560, but after that it begins to increase again and maintains itself at a near-equilibrium state. The Strouhal frequency of the vortex shedding at this near-equilibrium state is 0.1171 as compared to the natural vortex shedding Strouhal frequency 0.1654. This behavior has been suggested by Monkewitz in his theoretical work. He suggested that the wake stabilization might only be possible near the onset of shedding in a gain window between the suppression of the first mode and the destabilization of the higher mode. Recently, Roussopoulos [15] has experimentally observed a similar behavior at Reynolds number Re=52.8.

5 Experimental Results

The open loop response of the lift to the forcing of the suction/blowing actuators was studied first. The open loop forcing response was principally studied to provide some insight in the design of a closed loop control system. Also of interest was an examination of the "receptivity" and "lock-in" regions for open loop wake

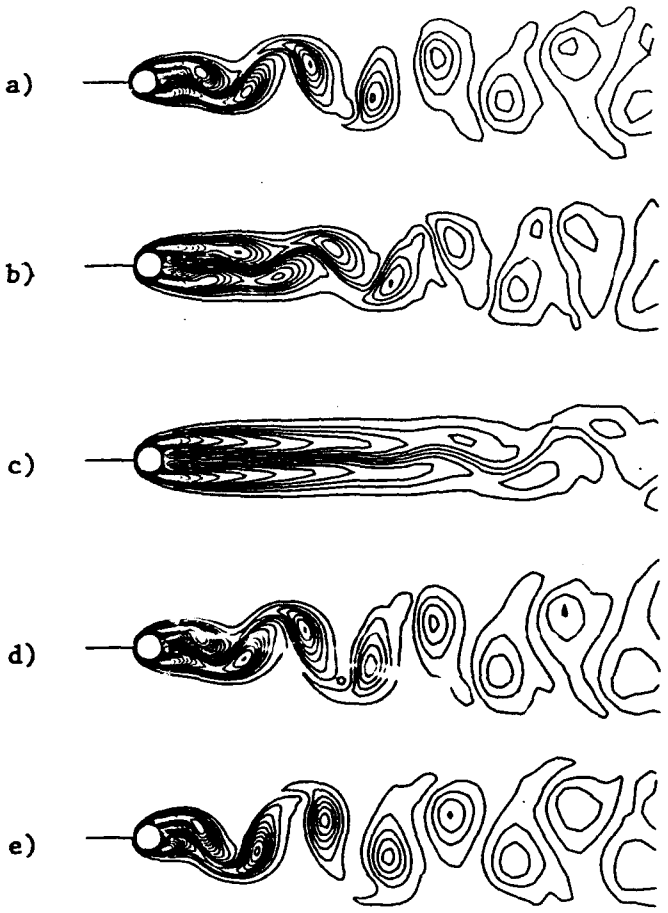

Figure 4: Vorticity contour plot at Re=80 corresponding to figure 3. a) t=43.04, b) t=170.9, c) t=243.58, d) t=452.89, e) t=640.3.

forcing discussed by Karniadakis & Triantafyllou[20]. In this context lock-in implies that the shedding frequency adjusts itself so that it exactly matches the forcing frequency. For large forcing amplitudes, the range of frequencies over which the shedding frequency follows the forcing frequency becomes larger. Receptivity on the other hand is defined as that region in the two dimensional forcing frequency-amplitude space, where the wake responds to the forcing in some manner, but does not actually adjust its frequency to match the forcing frequency. This region is larger and surrounds the lock-in region.

For both the open loop and closed loop tests a freestream velocity of 0.745m/sec was chosen. At this velocity the load cells produced a sufficiently large signal for use as feedback, and the natural shedding frequency was fairly low at about 11.3Hz, which was well within the proportional response range of the pump/motor combination. All results presented are nondimensionalized using the quantities nondimensional frequency = fd/U_∞, forcing coefficient v/U_∞, lift coefficient C_L and Reynolds number Re.

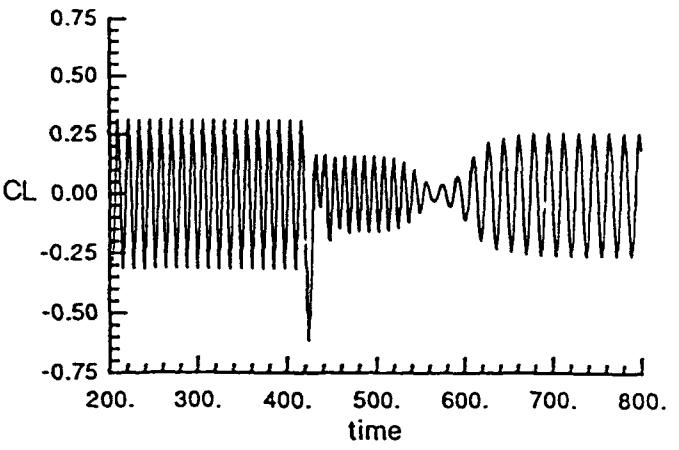

Figure 5: Lift coefficient at Re=100. Feedback forcing (x_s=5.05, α=0.3) is turned on at t=422.

Figure 6 is a waterfall display of the nondimensional linear spectrum of the lift coefficient, as the suction/blowing forcing frequency is stepwise (81 steps) increased from $fd/U_\infty = 0.135$ to 0.22. Here the peak forcing amplitude is $v/U_\infty = 0.04$, a relatively small amount of forcing. The forcing frequency shows as a diagonal peak in the waterfall display, starting at the lower left corner and advancing toward the upper right. The natural shedding frequency shows as a continuous ridge at $fd/U_\infty \approx 0.197$. At this low forcing level($v/U_\infty = 0.04$) the natural shedding is only slightly affected. The only response appears at the odd frequency of $fd/U_\infty \approx 0.17$, where careful examination shows a very small response in all the natural spectrums. This data indicates that this level of forcing is below the "threshold" postulated by Karniadakis & Triantafyllou[20]. Note that the momentum flux of the flow through the slots itself will produce a force reading on the load cells. The relative magnitude of this reaction force was tested by stepping through the test frequencies with no flow in the test section. In general this reaction force was at least an order of magnitude less than the forces induced with flow over the cylinder and is essentially independent of frequency. The second harmonic of the forcing frequency, which shows in the lower right hand quarter of the waterfall graphs is apparently an artifact of the reaction forces.

At a higher forcing amplitude in figure 7, as the forcing frequency approaches the natural frequency it can be observed that at $fd/U_\infty \approx 0.194$, the shedding frequency jumps to a lower frequency to coincide with the forcing frequency. This would be the left side of the

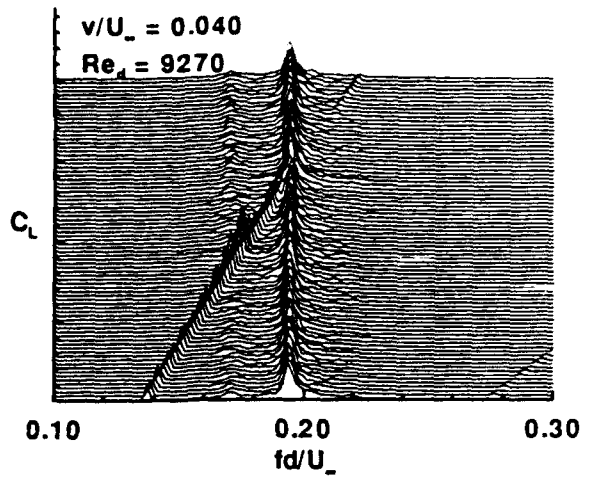

Figure 6: Waterfall plot of lift coefficient spectrum at a peak suction/blowing forcing of $v/U_\infty = 0.04$. Forcing frequency is discretely swept from $fd/U_\infty = 0.136$ to 0.22. Each spectrum is averaged 20 times.

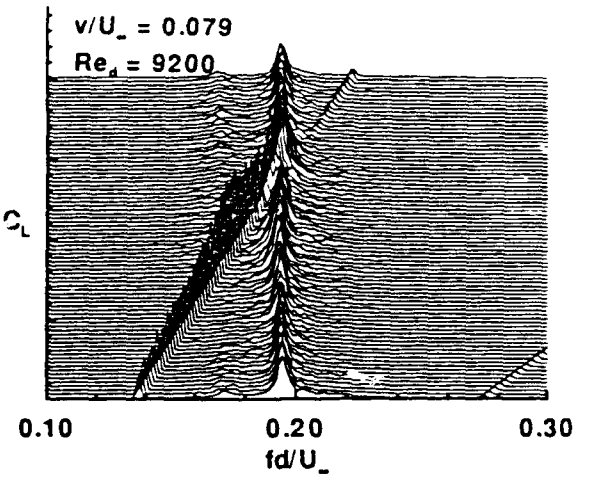

Figure 7: Same as figure 6, with suction/blowing forcing of $v/U_\infty = 0.079$.

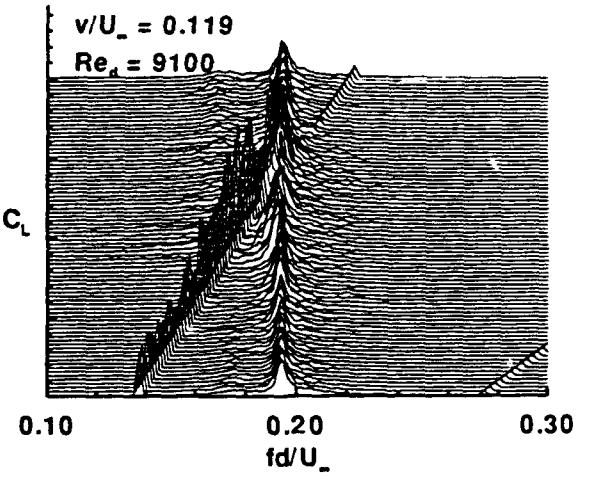

Figure 8: Same as figure 6, with suction/blowing forcing of $v/U_\infty = 0.119$.

lock-in region. Not readily apparent from figure 7 (but nontheless apparent on individual examination of the spectrums) is an area of sympathetic response at both the forcing frequency and the natural frequency, where the response amplitude for both peaks is increased. This may correspond to the receptive region of Karniadakis & Triantafyllou[20]. Their numerical results indicate that the induced response in this receptive region was the shedding frequency jumping back and forth between the forcing and the natural frequency, rather than the coexistence of two distinct frequencies. Our observations did not suggest this, as the time trace of the lift (in this response region), looked very much like the typical superposition of two frequencies. This would generally be a modulated sine wave with the modulation ("beat") frequency equal to the difference of the two basic frequencies. One further observation is that at forcing frequencies higher than natural, there is almost no response at all.

Figures 8 and 9 are similar to figure 7 with yet higher amplitude forcing. The trends at the higher forcing level are consistent with previous observations. At these higher forcing levels the lock-in and receptive regions are larger. However, there is still little response to forcing at higher than the natural frequency. In figure 9 close observation of the natural frequency ridge shows a slight bending of the natural frequency, towards the forcing frequency, as the lock-in region is approached from below. Figure 10 shows the "frequency response" of this system at two forcing levels ($v/U_\infty = 0.06$ and $v/U_\infty = 0.14$). Here the term frequency response is used in the linear system sense. The curves in figure 10 represent the output of the system (C_L at the forcing frequency) divided (as complex numbers) by the input (v/U_∞) as a function of forcing frequency. The response is represented as a complex number with both magnitude and phase. Linear response systems are characterized by magnitude and phase responses independent of input level. The curves in figure 10 represent the "vector" average of 20 spectrums for each of 81 response values. Vector averaging is analogous to ensemble averaging of time series, except performed in the frequency domain. Interesting aspects of figure 10 are: 1) The change of phase of the response is independent of forcing level. 2) Phase change is large in the region near the natural frequency. 3) Amplitude response is not directly proportional to forcing (not surprising for a nonlinear system). 4) The peak response for the lower level forcing is close to the natu-

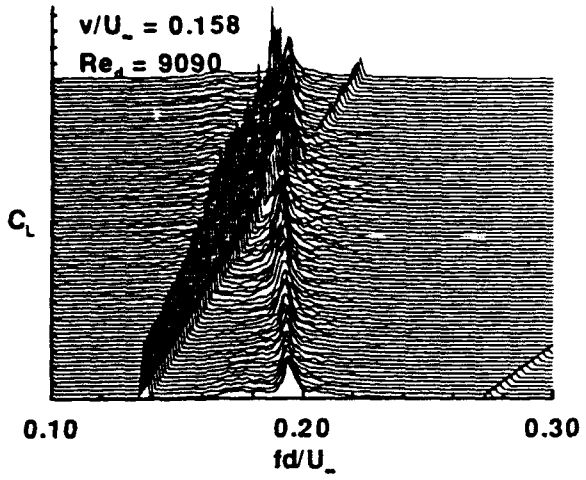

Figure 9: Same as figure 6, with suction/blowing forcing of $v/U_\infty = 0.158$.

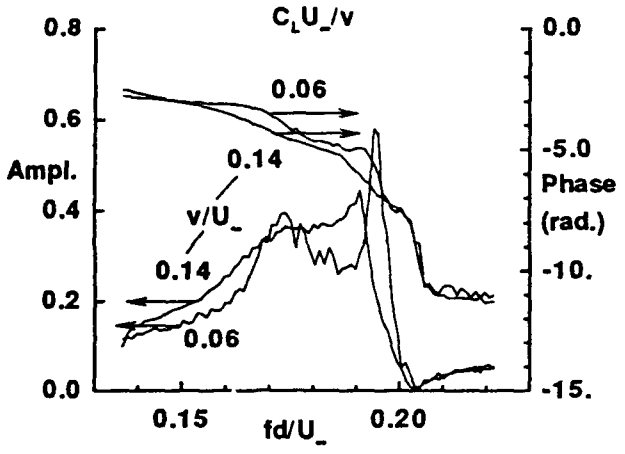

Figure 10: Lift coefficient response $C_L U_\infty / v$ (amplitude and phase) at the forcing frequency, with suction/blowing peak forcing velocity of $v/U_\infty = 0.14$ and 0.06.

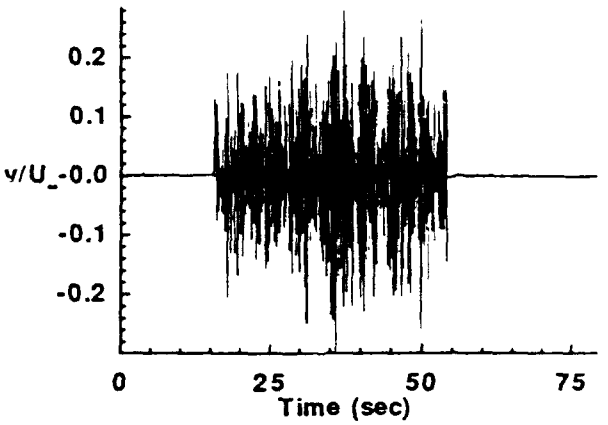

Figure 11: Closed loop forcing using PD feedback, with control turned on at 15 seconds and turned off at 55 seconds.

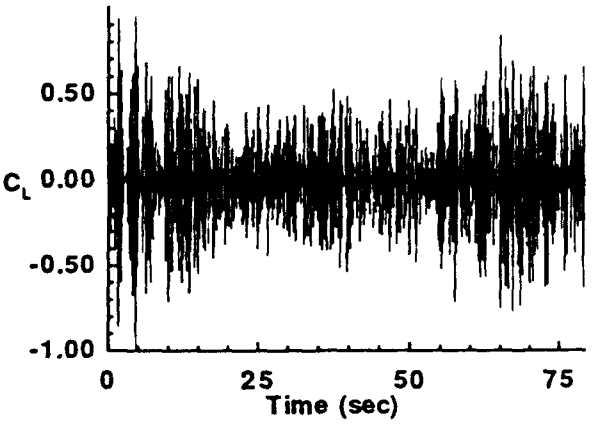

Figure 12: Response of lift coefficient, same conditions as figure 11.

ral frequency. The higher level forcing moves the peak response to a slightly lower frequency. This is the bending of the natural frequency referred to previously in the discussion of figure 9. 5) A receptive response region occurs at $fd/U_\infty \approx 0.17$.

The independence of the phase response to forcing level (noted in figure 10) suggests that perhaps a strictly linear feedback law could be used to control the level of unsteady lift forces. As a first cut, an IBM clone microcomputer was programmed to serve as a PID (proportional, integral and derivative) controller. Input to the control loop was the (amplified and antialiased) average of the top and bottom load cell lift forces. C put was an analog voltage to drive the pump servomotor. Parameters of the PID loop were manually adjusted to effect the desired results. Here the loop error was taken to be any lift force different from zero. The integral term of the PID loop was set to zero, as this term controls the steady state error of the lift, generally of no concern for this study. Figure 11 shows the nondimensionalized control signal to the pump, as the "best" manually adjusted control loop is first turned on and then off. Figure 12 is the corresponding long term response of the (top) lift force as the the control is turned on and off. The results are not spectacular, but the reduced level of unsteady lift in the middle section of the trace of figure 12 represents a 50% reduction of the rms level of lift force. The parameters of the control loop also could be set to enhance the unsteady lift forces, however the response level of the system was so

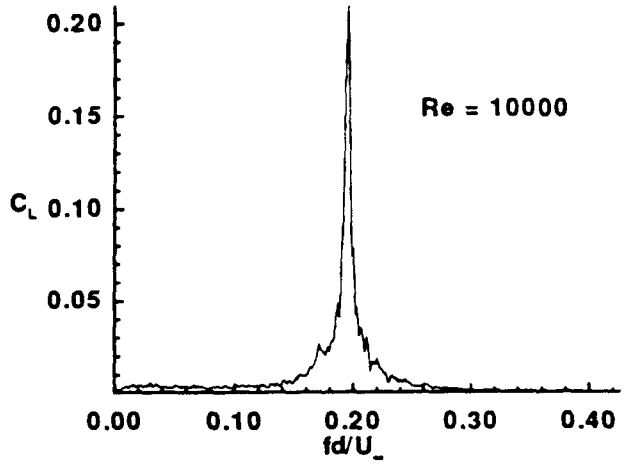

Figure 13: Averaged spectrum of lift coefficient, without any control. Same conditions as the no control case of figure 12.

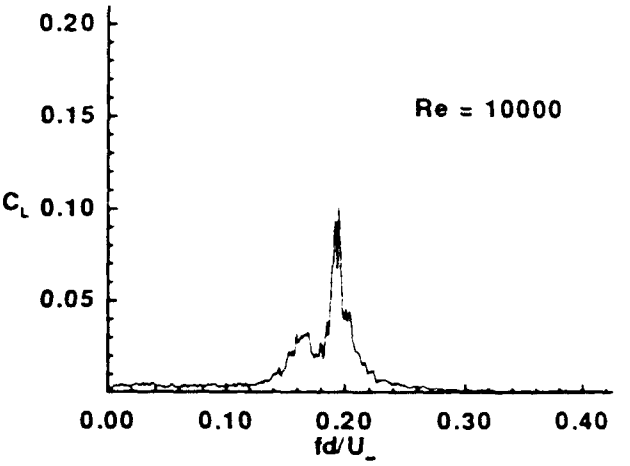

Figure 14: Averaged spectrum of lift coefficient, with control. Same conditions as the control on case of figure 12.

high as to cause concern for the mechanical integrity of the pump system and these results were not pursued.

Figure 13 shows the spectrum of lift response before control is applied and figure 14 is taken during the period when the control loop is operative. In figure 14 it is observed that in addition to the reduction of the level of the natural shedding frequency, an enhanced response is appearing at $fd/U_\infty = 0.17$. In the process of the averaging of the spectrum of figure 14, it was observed that the system was alternately jumping between the natural frequency and the new preferred frequency of 0.17. This is in contrast to the open loop response to forcing, which can be characterized as the coexistence of two distinct frequencies. This behavior can be compared with the numerical results of figure 5. Here the flow with feedback has chosen a new (lower) shedding frequency. Again, this behavior is similar to observed behavior of the systems in Monkewitz [16], Monkewitz et al. [17] and Roussopoulos [15]. We believe this behavior to be endemic of linear control systems applied to nonlinear systems of this type, at high supercriticality (e.g. high Reynolds number).

6 Conclusions

The computational study of the feedback control of the Kármán vortex shedding behind a circular cylinder has been undertaken at low Reynolds numbers. Two-dimensional Navier-Stokes equations are solved numerically. The actuators are a pair of blowing/suction slots located at $\pm 110°$ from the leading stagnation point. A single sensor is used and the actuators are out of phase with each other. Complete suppression of vortex shedding is achieved up to Reynolds number Re=80, which is about 70% above the onset Reynolds number of vortex shedding. At Re=100 the feedback suppression destabilizes a second mode.

Closed loop feed back stabilization has been used to suppress lift fluctuation at Reynolds number Re=10,000 up to 50% over the natural conditions. Although the experiments that were performed were done at a much higher Reynolds number than the simulations, many of the salient features of the two studies were similar. The open loop response of the cylinder to high amplitude forcing (Figure 9) exhibited a slight bending of the natural frequency, towards the forcing frequency, as the lock-in region is approached from below. This observation is similar to some numerical results of one of us (Park) with open loop suction/blowing forcing at $Re = 120$. We believe this to be related to a change of the wake structure (wider), such that the preferred shedding frequency is lowered. In addition, the destabilization of a second instability by the feedback control was noted in the experiments and mirrored in the simulations.

We would like to acknowledge the support of the ONT (Office of Naval Technology) Postdoctoral Fellowship to one of us (Daniel Park).

References

[1] T. Sarpkaya. Vortex-induced oscillations. *J. Appl. Mech.*, 46:241-258, 1979.

[2] P. W. Bearman. Vortex shedding from oscillating bluff bodies. *Ann. Rev. Fluid Mech.*, 16:195, 1984.

[3] G. H. Koopmann. The vortex wakes of vibrating cylinders at low Reynolds numbers. *J. Fluid Mech.*, 28:501, 1967.

[4] O. M. Griffin and S. E. Ramberg. The vortex street wakes of vibrating cylinders. *J. Fluid Mech.*, 66:553, 1974.

[5] B. J. Armstrong, F. H. Barns, and I. Grant. The effect of a perturbation on the flow over a cylinder. *Phys. Fluids*, 29:2095, 1986.

[6] A. Ongorin and D. Rockwell. Flow structure from an oscillating cylinder: Part 1. Mechanisms of phase shift and recovery in the near wake. *J. Fluid Mech.*, 191:197, 1988.

[7] A. Ongorin and D. Rockwell. Flow structure from an oscillating cylinder: Part 2. Mode competition in the near wake. *J. Fluid Mech.*, 191:225, 1988.

[8] P. T. Tokumaru and P. E. Dimotakis. Rotary oscillation control of a cylinder wake. *J. Fluid Mech.*, 224:77, 1991.

[9] J. R. Filler, P. L. Marston, and W. C. Mih. Response of the shear layers separating from a circular cylinder to small amplitude rotational oscillations. Submitted to *J. Fluid Mech.*, 1991.

[10] J. Mo. An investigation on the wake of a cylinder with rotational oscillations. Ph.D. thesis, Univ. of Tennessee Space Institute, 1989.

[11] Y. M. Chen, Y. R. Ou, and A. J. Pealstein. Development of the wake behind a circular cylinder impulsively started into rotatory and rectilinear motion: intermediate rotation rates. *ICASE Report*, 91-90, 1991.

[12] R. D. Blevins. The effect of sound on vortex shedding from cylinders. *J. Fluid Mech*, 161:217, 1985.

[13] E. Detemple-Laake and H. Eckelmann. Phenomenology of Kármán vortex streets in oscillatory flow. *Exp. Fluids*, 7:217, 1989.

[14] E. Ffowcs Williams and B. C. Zhao. The active control of vortex shedding. *J. Fluids Struct.*, 3:11, 1989.

[15] K. Roussopoulos. Feedback control of vortex shedding at low Reynolds numbers. *J. Fluid Mech.*, 248:267, 1993.

[16] P. A. Monkewitz. Feedback control of global oscillations in fluid systems. *AIAA paper*, 89-0991, 1989.

[17] P. A. Monkewitz, E. Berger, and M. Schumm. The nonlinear stability of spatially inhomogeneous shear flows, including the effect of feedback. *Eur. J. Mech. B Fluids*, 10:295, 1991.

[18] D. S. Park, D. M. Ladd, and E. W. Hendricks. Feedback control of Kármán vortex shedding behind a circular cylinder at low Reynolds numbers. Submitted to *Phys. Fluids A*, 1993.

[19] G. E. Karniadakis, M. Israeli, and S. A. Orszag. High-order splitting methods for the incompressible Navier-Stokes equations. *J. Comput. Phys.*, 97:414, 1991.

[20] G. L. Karniadakis and G. S. Triantafyllou. Frequency selection and asymptotic state in laminar wake. *J. Fluid Mech.*, 199:441, 1989.

[21] C. H. K. Williamson. Oblique and parallel modes of vortex shedding in the wake of a circular cylinder at low Reynolds numbers. *J. Fluid Mech.*, 206:579, 1989.

[22] B. Fornberg. A numerical study of steady viscous flow past a circular cylinder. *J. Fluid Mech.*, 98:819, 1980.